

Research  
High-End Measuring Instruments—Review

## Fluorescence Nanoscopy in Neuroscience

Yangyundou Wang, Jian Lin, Qiming Zhang, Xi Chen, Haitao Luan, Min Gu\*



Center for Artificial-Intelligence Nanophotonics, School of Optical-Electrical and Computer Engineering, University of Shanghai for Science and Technology, Shanghai 200093, China

### ARTICLE INFO

#### Article history:

Received 4 July 2020

Revised 17 September 2020

Accepted 30 November 2020

Available online 21 May 2021

#### Keywords:

Fluorescence imaging

Diffraction limit

Nanoscale resolution

Neuroscience

### ABSTRACT

Fluorescence nanoscopy provides imaging techniques that overcome the diffraction-limited resolution barrier in light microscopy, thereby opening up a new area of research in biomedical imaging in fields such as neuroscience. Here, we review the foremost fluorescence nanoscopy techniques, including descriptions of their applications in elucidating protein architectures and mobility, the real-time determination of synaptic parameters involved in neural processes, three-dimensional imaging, and the tracking of nanoscale neural activity. We conclude by discussing the prospects of fluorescence nanoscopy, with a particular focus on its deployment in combination with related techniques (e.g., machine learning) in neuroscience.

© 2022 THE AUTHORS. Published by Elsevier LTD on behalf of Chinese Academy of Engineering and Higher Education Press Limited Company. This is an open access article under the CC BY-NC-ND license (<http://creativecommons.org/licenses/by-nc-nd/4.0/>).

## 1. Introduction

The scope of neuroscience [1] includes the scientific study of the organization of the nervous system and its function in generating behavior. From a macroscopic perspective, neural systems comprise neurons and circuits that are distributed in a number of discrete anatomical locations in the brain and subservise one of three general functions: sensory, motor, and association. At the nanoscopic scale, the organization of synapse-associated proteins is critical for the stability and function of neuronal processes, such as neuronal transmission. For example, during signal transmission at chemical synapses, the elevation of the presynaptic  $\text{Ca}^{2+}$  concentration caused by the arrival of the action potential (AP) (associated with synaptotagmin) leads to neurotransmitter release after the soluble *N*-ethylmaleimide sensitive factor attachment protein receptor (SNARE) complex has brought the two membranes together [2,3]. An elaborate protein-based cytomatrix plays an important role during the release process. Clathrin is also involved in the endocytic budding of vesicles from the plasma membrane [4].

In addition to protein mobility, protein distribution plays diverse functional roles in neuronal signaling. For example, the information conveyed by synapses in the form of the excitatory postsynaptic current (EPSC) or inhibitory postsynaptic current (IPSC) is integrated and “read out” at the origin of the axon. Fur-

thermore, the EPSC model reflects the initial size of the readily releasable pool and its replenishment rate from a reserve pool, the probability of synaptic vesicle (SV) release, and synaptic facilitation [5]. An axon has a distinct cytoskeleton containing proteins such as actin and spectrin, along with associated proteins that affect its functional integrity. The membrane-associated periodic skeleton (MPS) potentially influences the generation and propagation of APs and other signaling pathways in axons.

Fluorescence microscopy is the most prevalent imaging technique in the field of biology due to its advantages with respect to molecule-specific labeling using fluorescence tagging and its real-time imaging ability. Owing to the diffraction limit of light, it is impossible to resolve protein mobility and subcellular structures such as synapses at the nanoscale level using conventional light microscopy. In recent years, several forms of fluorescence nanoscopy have emerged that enable imaging at 2–100 times the resolution of conventional fluorescence microscopy [6–16]. Fluorescence nanoscopy offers a powerful new imaging tool with a resolution similar to that of electron microscopy; at the same time, it has certain advantages suited to investigating subcellular structures and biological processes, including live-cell, multicolor, real-time, and three-dimensional (3D) molecular imaging, as well as tracking capabilities [17]. Combined with other cutting-edge techniques, fluorescence nanoscopy provides a route to better understand the function of neurons, neuronal circuits, and, ultimately, neural systems.

In this review, we summarize several fluorescence nanoscopy techniques: structured illumination microscopy (SIM), stimulated

\* Corresponding author.

E-mail address: [gumin@usst.edu.cn](mailto:gumin@usst.edu.cn) (M. Gu).

emission depletion (STED) microscopy, stochastic optical reconstruction microscopy (STORM)/photoactivatable localization microscopy (PALM), and minimal photon fluxes (MINFLUX) nanoscopy, which incorporates both STED microscopy and STORM. Then, we discuss advanced applications of these techniques from the perspective of molecular and cellular neuroscience. Finally, we conclude by considering the prospects of fluorescence nanoscopy in neuroscience.

## 2. Fluorescence and the diffraction limit

### 2.1. The principle of fluorescence

A fluorophore is a fluorescent chemical compound that can absorb photons in the “ground state,” leading to fluorescence emission and vibration relaxation in the “excited state.” The transition from ground state to excited state occurs very rapidly (over femtoseconds). One of the most useful approaches for understanding the emission and absorption processes is the Jablonski diagram (Fig. 1). The singlet states are caused by the cancellation of the magnetic moments of electrons that have opposite spins within a single state. The triplet states are relatively long-lived.  $S_0$  denotes the ground state, with  $S_1$  and  $S_2$  representing excited singlet states.  $S_2$  is a higher energy state than  $S_1$ , whereas  $S_0$  is a lower energy state than  $S_1$ .

Because of the Stokes shift of fluorescence, that is, the red-shifted wavelength of the emitted light relative to the absorbed light, the contrast between the signal-to-background ratio in fluorescence microscopy has been improved dramatically [18]. Furthermore, the basic principle of fluorescence microscopy—namely, illuminating the stained sample with the excitation wavelength and detecting its fluorescence signal at a longer emission wavelength—is easy to understand.

### 2.2. Impact of the diffraction limit

A light microscope can be regarded as a lens system that can be utilized to visualize fine structures in a specimen. As light is a wave that can be diffracted, the 3D point spread function (PSF) produced by a point object has a finite size. Based on constructive interference in space, the full width at half maximum (FWHM) of the PSF is  $\Delta r \approx \lambda / (2n \times \sin \alpha)$  in the focal plane and  $\Delta l \approx \lambda / (n \times \sin^2 \alpha)$  along the optical axis. Here,  $\lambda$ ,  $\alpha$ , and  $n$  denote the wavelength of

light, the aperture angle of the objective, and the refractive index of the immersion medium, respectively;  $\Delta r$  is FWHM of the PSF in the lateral directions;  $\Delta l$  is FWHM of the PSF in the axial directions. As shown in Fig. 2, when imaging with visible light ( $\lambda = 632.8$  nm) and an oil immersion objective with a numerical aperture (NA) of 1.40 ( $NA = n \times \sin \alpha$ ), the lateral size of the PSF is approximately 226 nm and the axial size of the PSF is approximately 487 nm. The limited diffraction of light results in unresolvable molecular structures, such that the nanoscale fundamental mechanisms in cells remain invisible.

## 3. Fluorescence nanoscopy techniques

Since the mid-20th century, several concepts, including confocal fluorescence microscopy [19] and multi-photon microscopy [20], have been introduced to reduce the out-of-focus fluorescence background and the capability of optical sectioning. In principle, confocal fluorescence microscopy improves the spatial resolution by a factor of  $\sqrt{2}$  compared with conventional fluorescence microscopy. In practice, they are the same because of the finite detector size. Confocal one- and two-photon fluorescence microscopy techniques provide almost identical resolution. By expanding the illumination or detection wavefront, the 4Pi microscope can achieve lateral resolutions between 80 and 150 nm in fixed cells [21]. Based on the Moiré effect, SIM shifts the high-frequency features to low frequencies, which can be detected by the microscope. SIM offers 100–120 nm lateral resolution and about 300 nm axial resolution. However, the resolution remains limited by the diffraction of light.

Regarding fluorophore photophysics and photochemistry, the techniques that have achieved the most remarkable breakthroughs are STED microscopy and STORM/PALM, both of which have broken the diffraction barrier by reading out the molecular fluorescence features of the diffraction zone sequentially. To be specific, reading out markers refers to the signal providing a “bright state” while keeping other markers in the “dark state” [22]. Recently, combining the strengths of both techniques, MINFLUX nanoscopy has offered a more powerful and versatile imaging tool for biological studies, achieving resolutions of 1–3 nm in fixed and living cells [16]. Fig. 3 shows the imaging principles of SIM, STED microscopy, STORM/PALM, and MINFLUX nanoscopy. Similar to STORM/PALM, MINFLUX nanoscopy relies on imaging single (or at least identifiable) molecules at a time. In other words, as opposed to MINFLUX nanoscopy and STORM/PALM, STED microscopy principally reads

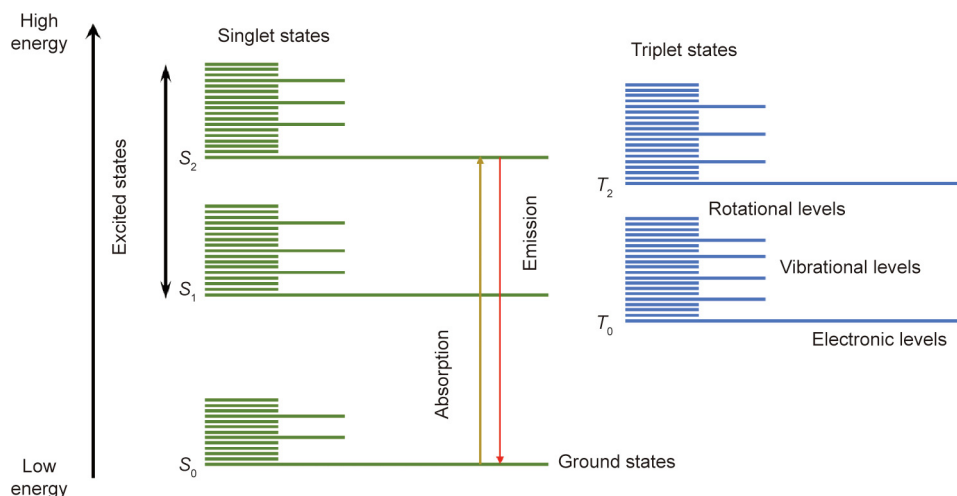
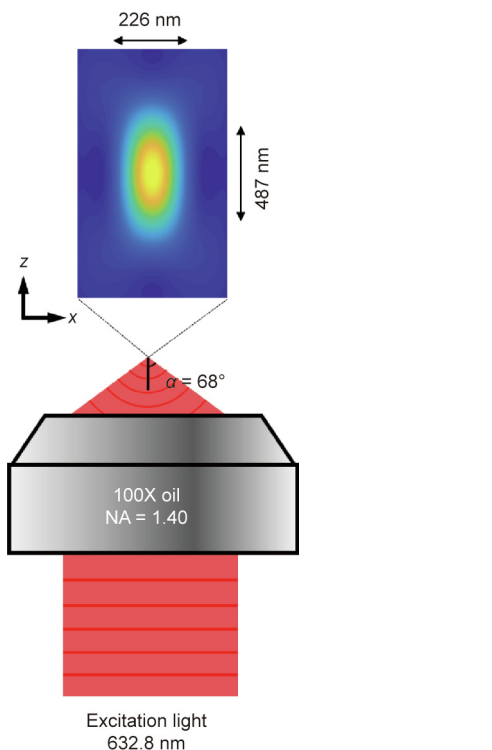


Fig. 1. Jablonski diagram illustrating the energy states within a fluorescence molecule.  $S_0$  is the ground state;  $S_1$  and  $S_2$  are the excited singlet states;  $T_0$  and  $T_2$  are the triplet states.



**Fig. 2.** PSF of an oil immersion objective with NA = 1.40. The excitation wavelength is 632.8 nm. NA: numerical aperture.

out fluorescence ensembles, relying on reversible transitions between the dark and bright states.

### 3.1. Structured illumination microscopy

Using a pattern illumination field, SIM [6] combines optical manipulations and computational algorithms to obtain optical sections and facilitate 3D imaging. In the spatial domain, the observed data  $D$  in a linear-invariant optical system can be expressed as a convolution of the emitting object  $E$  and the PSF  $H$ :  $D(r) = E(r) \otimes H(r)$ , where  $r$  is localization position. By contrast, the convolution can be expressed in the Fourier domain as a point-wise product,  $D(k) = \widetilde{E}(k) O(k)$ , where  $O$  is the optical transfer function (OTF) and  $k$  is the spatial frequency. The OTF defines the spatial frequency or observable region that can be detected by the microscope. As shown in Fig. 3 the resolution of a reconstructed image of the emitting object can be improved in both the lateral and axial directions using a sum of periodic illumination patterns with different phases and orientations [7,8].

### 3.2. STED microscopy

In the 1990s, the concept of STED microscopy was proposed for propagating light and regular lenses in the far field [9,10]. Using time-sequential patterned illumination, it is the most direct way to determine the coordinates of bright markers. This technique can be regarded as a reversible saturable optically linear fluorescence transition (RESOLFT). In addition to STED microscopy,

	Acronyms proposed/verified	Principle	Resolution
Photophysics	SIM 1993/2000	Moiré fringes 	100–120 nm (in lateral)
Photophysics	STED microscopy 1994/1999		$\frac{\lambda}{2n \sin \alpha \sqrt{1 + \frac{I}{I_s}}}$ Ensemble
Photochemistry	STORM/PALM 2006		$\frac{\lambda}{2n \sin \alpha \sqrt{N}}$ 1 molecule
Photochemistry photophysics	MINFLUX nanoscopy 2017		$\frac{L}{1 + \sqrt{n_1 n_0}}$ (1D) 1 molecule

**Fig. 3.** Working principle and resolution of SIM, STED microscopy, STORM/PALM, and MINFLUX nanoscopy. Using a sinusoidal illumination pattern, SIM can recover information that is twice the size of the normal observation region in the Fourier domain. In other words, SIM obtains twice the normal resolution in the spatial domain (100–120 nm). A typical single-point scanning STED microscope quenches the excitation beam (blue) using a doughnut-shaped STED beam (orange). PALM and STORM read out individual molecules stochastically.  $N \gg 1$  photons permits the centroid calculation for individual molecules within the diffraction spot. The purple blob represents a diffraction spot that is given the range of the target (the white star). Using an adjustable doughnut-shaped beam, the targeted coordinate pattern comprises four designated coordinates (shown as black, red, yellow, and blue circles).  $I$ : the peak intensity of the “STED beam”;  $I_s$ : the saturation intensity of the fluorophore;  $N$ : the number of photons at the fluorophore position;  $L$ : doughnut pattern size;  $n_0$  and  $n_1$  are the fluorescence photons counted for doughnut position  $r_0$  and  $r_1$ , respectively; 1D: one-dimension;  $r_0, r_1, r_2,$  and  $r_3$  are doughnut positions, respectively.

RESOLFT refers to ground-state depletion microscopy [10]. As shown in Fig. 3, based on the confocal microscopy configuration, fluorescence markers are excited by a focused excitation beam. Within the spontaneous decay of fluorophores, the overlap of the excitation and STED microscopy beams yields sub-diffraction spots. The practical resolution of STED microscopy is  $\Delta r \approx \lambda / (2n \sin \alpha \sqrt{1 + I/I_s})$ . Here,  $I$  is the peak intensity of the “STED beam” and  $I_s$  is the saturation intensity of the fluorophore. In order to improve the resolution, the intensity of a redshifted doughnut-shaped STED beam produced by a spiral spatial phase modulator or vortex phase plate must satisfy  $I > I_s$ . In other words, the resolution of STED microscopy is determined solely by the STED beam. By increasing the intensity of the STED beam, the diameter of effective spots is restricted to a lateral resolution of 20 nm. Nonetheless, suitable dyes and adaptive illumination must be adopted in order to avoid photobleaching.

### 3.3. STORM/PALM

In contrast to the chosen coordination in STED microscopy, in STORM [11], PALM [12,13], and points accumulation for imaging in nanoscale topography (PAINT), single fluorescent molecules are read out from random coordinates (Fig. 3). Using wide-field illumination, a single molecule is switched on or activated. The next activated molecule is a distance of  $\lambda/2n$  from the former activated molecule. The repeated excitation of molecules forms a magnified diffraction spot on the camera. The image is then assembled molecule by molecule via a dark–bright–dark state mechanism for both switching and non-switching fluorophores. The detected photons enable the localization of the centroid position of the spot and determine the lateral position of the molecules. The optical resolution of STORM/PALM is approximately  $\lambda / (2n \sin \alpha \sqrt{N})$ , where  $N$  is the number of photons at the fluorophore position. It should be mentioned that high-quality STORM images require fluorophores with a high photon yield per switching event, low on–off duty cycle, high survival fraction, and several switching cycles. Among these properties, a low on–off duty cycle leads to the maximum fluorophore density, which equates to achieving the maximum imaging resolution permitted by the Nyquist criterion. However, the activation light does not change the number of detected photons per switching event.

### 3.4. MINFLUX nanoscopy

In 2017, a localization concept called MINFLUX nanoscopy was proposed by Stefan Hell’s laboratory [14–16]. This technique combines patterned illumination with single-molecule features (as in STORM/PALM) to obtain the coordinates of the target molecules (as in STED microscopy). MINFLUX nanoscopy has advanced 3D multicolor molecular imaging and tracking into the hitherto unrealized regime of single-digit nanometer precision and approximately 100  $\mu$ s time resolution in a scalable field of view (FOV). As shown in Fig. 3, MINFLUX nanoscopy employs a movable excitation beam with an intensity minimum at its center. This minimum serves as a reference coordinate, with the number of emitted photons decreasing as it approaches the fluorophore. Therefore, unlike STED microscopy and STORM/PALM, MINFLUX nanoscopy does not require a large number of photons.

The MINFLUX nanoscopy setup consists of an activation beam that activates fluorophores within the approximately 400 nm activation region and an excitation beam that localizes or tracks the molecules. For each localization, the beam is first focused regularly; then, a modulated two-dimensional (2D) or 3D doughnut pattern, with a gradually shrinking diameter ( $L$ ), is positioned to localize or track molecules through their maximum-likelihood estimation in either the focal plane ( $x, y$ ) or the sample volume ( $x, y, z$ ). In

one dimension, the minimum standard deviation of the localization, that is, the Cramer–Rao bound (CRB) within the region  $L$ , is  $\sigma \geq L / (4\sqrt{N})$ , where  $\sigma$  is the localization position,  $N = n_1 + n_0$  is the number of detected photons at different locations ( $r_1$  and  $r_0$ ) in the doughnut pattern. Within the activation area, a localization precision of  $(\sigma - 1)$  nm in one dimension can be expected with only  $N = 600$  photons. Therefore, the iteration precision of MINFLUX nanoscopy surpasses the quantum CRB (QCRB) of the lateral precision for camera-based localization.

Aside from fluorescence nanoscopy, which directly overcomes the diffraction limit of light, expansion microscopy (ExM) can achieve nanoscale 3D imaging, even when using conventional diffraction-limited microscopes, through the physical magnification of tissue and organ specimens [23]. Over the past few years, various ExM protocols have been proposed for the high-resolution imaging of proteins [24] and ribonucleic acids (RNAs) [25], or for application in human clinical specimens [26]. In order to achieve isotropic specimen expansion, biomolecules and/or labels are first mechanically coupled to the polymer mesh. The specimen is then homogenized and expanded. The resolution of ExM can reach the subcellular level with two rounds of expansion using CUBIC-X, which is based on an aqueous chemical solution [27].

## 4. Imaging capabilities of fluorescence nanoscopy

In the last few decades, fluorescence nanoscopy has become more suitable for the imaging of subcellular dynamics and structures in three dimensions, multiple colors, and living systems with nanometer-scale resolution. Consider commercial STED as an example: The STED INFINITY (Abberior Instruments, Germany) line can reach a lateral resolution of  $< (20 \text{ nm} \times 20 \text{ nm})$  and  $< (70 \text{ nm} \times 70 \text{ nm} \times 70 \text{ nm})$  in two and three dimensions, respectively. Coupled with a 100X objective lens, the FOV is  $80 \mu\text{m} \times 80 \mu\text{m}$ . Using Quadscanner (Abberior Instruments), the line frequency can be as high as 2.6 kHz and data collection can reach 4.2 frames per second for  $512 \text{ pixel} \times 512 \text{ pixel}$ . An imaging depth of up to 100  $\mu\text{m}$  can be achieved inside a complex sample such as *Drosophila* larvae using adaptive optics. In order to reduce photobleaching and phototoxicity, the STED with Dymin imaging mode simultaneously minimizes the light dose and enhances the signal by an order of magnitude.

The tradeoff between spatial and temporal resolutions is essential in high-resolution imaging techniques, especially in fluorescence nanoscopy. STED can image a relatively small FOV with millisecond temporal resolution [28]. Equipped with fast-switching dyes [29] and fast complementary metal-oxide semiconductor (CMOS) cameras [30], STORM microscope can achieve sub-second time resolution at about 20–30 nm spatial resolution for large FOVs in live-cell imaging. Moreover, photobleaching and/or phototoxicity can be decreased drastically in STED microscope and STORM/PALM. With its low phototoxicity, patterned activation nonlinear SIM (PA NL-SIM) demonstrated live-cell imaging with approximately 60 nm spatial resolution and sub-second time resolution over large FOVs with tens of time points [31]. In MINFLUX nanoscopy, ultraprecise 2 nm spatial resolution and 100 kHz temporal resolution can be achieved with its minimal photon budget (i.e., low photobleaching/phototoxicity for fixed and living cells) and scalable FOV [16].

## 5. Applications of fluorescence nanoscopy in neuroscience

Although fluorescence nanoscopy delivers very fine structural information (e.g., a subcellular compartment of densely packed proteins) in the active zone (AZ), the specific physiological properties of different molecular architectures remain a major challenge [32]. Fluorescence nanoscopy is applied primarily to investigate

structure (e.g., MPS and function of proteins), especially in the synaptic button (e.g., presynaptic AZ and the postsynaptic density (PSD)). Because of the properties of tissue and light, dynamic, live-cell and *in vivo* deep tissue imaging remain challenging [17]. As STED microscopy offers live cell-tracking features, synaptic fusion during neuron transmission has been revealed dynamically.

### 5.1. Spatial organization of proteins in synapses

The protein-based cytomatrix at the AZ (CAZ) is crucial for facilitating the SV release process. The Rab subfamily Rab3-interacting molecule (RIM)-binding protein (RBP) is the primer effector of the AZ scaffold. Hence, the RBP family is essential for the coupling of SVs, Ca<sup>2+</sup> channels, and the SV fusion machinery in *Drosophila*. Two-color STED microscopy has demonstrated that the RBP-based cytomatrix has a direct function in controlling the number of readily releasable SVs. As shown in Fig. 4(a) [33], the *Drosophila* RBP (DRBP) surrounds the central Ca<sup>2+</sup> channel field. The DRBP is critical for the integrity of the AZ scaffold and for neurotransmitter release [33]. Moreover, according to direct STORM, the CAZ includes units that contain 137 Bruchpilot (Brp) proteins. The organization of these units relates to various AZ states that correlate to different neurotransmission release probabilities [34].

During neural transmission, SVs fuse within the AZ membrane in response to Ca<sup>2+</sup> influxes. In the core fusion complex, there are SNARE proteins, vesicle components, and AZ-specific proteins, all of which help SVs and membranes to dock and fuse. STED microscopy has been implemented to visualize the SNARE protein syntaxin [35], the unclear protein SC35 [36], and the nicotinic acetylcholine receptor [37].

Scaffolding proteins such as postsynaptic density protein 95 (PSD-95) [38], guanylate-kinase-associated protein [39], con-

densed Shank3 [40], and Homer [41] are major components of PSDs. STORM and PALM imaging have both mapped the spatial organization of proteins in the pre- and post-synaptic terminals, including the orientation of presynaptic scaffolding proteins, the laminar organization of PSDs, and the lateral distributions of neurotransmitter receptors [42–44]. Fig. 4(b) [42] shows the axial and radial 3D STORM images of presynaptic Bassoon (red) and postsynaptic Homer1 (green). It should be noted that PSD-95 plays a crucial role in anchoring and rearranging glutamate receptors in the postsynaptic membrane [38–41,45]. For example, using STED microscopy in combination with endogenous protein labeling, PSD-95 frequently appears in extended distributions rather than as isolated nanoclusters [46]. Recently, MINFLUX nanoscopy has suggested that PSD-95 is distributed along a slightly curved surface with a side length of 100–400 nm, as shown in Fig. 4(c) [16].

### 5.2. Cytoskeleton structures of axons

MPSs in axons were first discovered using STORM [47]. It was observed that short actin filaments capped by actin-capping proteins are organized into repeating ring-like structures as axon bundles. The adjacent actin rings are connected by spectrin tetramers, forming a long-range quasi-one-dimensional periodic structure. This structure is formed underneath the axonal membrane with a periodicity of approximately 180–190 nm. However, researchers using MINFLUX nanoscopy recently found that, at a spatial resolution < 2 nm, the MPS resembles a periodic spiral structure in the axon. In addition, using STED microscopy and STORM, the MPS in dendrites was observed [48,49]. However, the formation propensity and development rate of the MPS in dendrites appears to be lower than those in axons. Moreover, a 2D polygonal lattice structure formed by MPS components was observed in the soma, the

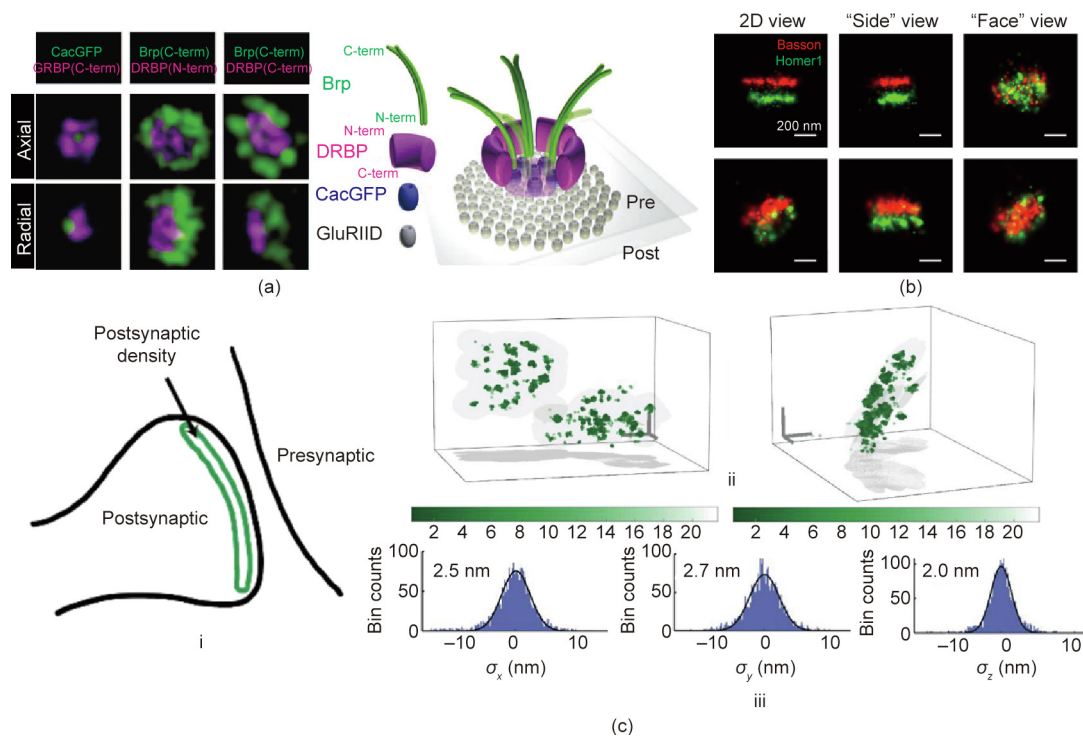


**Fig. 4.** Nanoscopic imaging of synaptic protein structures. (a) Left: 3D STED images of the presynaptic AZ containing DRBP, Brp, and the voltage-gated Ca<sup>2+</sup> channel cacophony (Cac) at neuromuscular junction synapses in *Drosophila*. Right: model of an AZ in oblique view. DRBP: *Drosophila* RBP; Brp: Bruchpilot; GFP: green fluorescent protein; CacGFP: GFP labelled Ca<sup>2+</sup> channels; GluRIID: glutamate receptors subunit. (b) 3D STORM images of synapses. (c) MINFLUX nanoscopy imaging of PSD-95 with 3D resolution of 2–3 nm. (i) Sketch of postsynaptic PSD-95. (ii) PSD-95 appearing as clusters distributed on a curved surface. (iii) Individual fluorophores with an isotropic 3D localization precision of 2.0–2.7 nm. PSD-95: postsynaptic density protein 95. (a) Reproduced from Ref. [33] with permission of The American Association for the Advancement of Science, © 2011; (b) reproduced o Ref. [42] with permission of Elsevier, © 2010; (c) reproduced from Ref. [16] with permission of Springer Nature, © 2020.

dendrites, and the node of Ranvier [48–53]. In other words, the structure of the MPS in neurons requires further elucidation in order to decipher its function in facilitating or assisting the generation and propagation of APs, which remains unclear thus far.

### 5.3. Temporal dynamics of vesicle fusion

It is known that the CAZ provides a functional platform for releasing SVs during neural transmission and communication. However, the principle of vesicle mobility was elusive prior to the invention of STED microscopy, which enabled the movements of SVs in hippocampal neurons to be tracked. The synaptotagmin was labeled with antibodies conjugated to Atto 647N (ATTO-TEC GmbH, Germany), and a final image with a spatial resolution of 62 nm was captured displaying an area of  $1.8 \mu\text{m} \times 2.5 \mu\text{m}$  at 28 frames per second [54]. This shows that vesicles continuously bind and then diffuse away from the cellular organelles in a manner similar to the “stick and diffuse” model. Furthermore, isoSTED microscopy has been used to track vesicles during two cycles of endocytosis and exocytosis, indicating that the same vesicles are used for release in both spontaneous and stimulated neurotransmitter release [55]. However, the underlying mechanism of vesicle trafficking remains unknown. STED microscopy has also resolved synaptotagmin I from individual SVs that form isolated clusters upon vesicle fusion. By labeling synaptotagmin with sheep anti-mouse Atto 532 dye, STED microscopy realized a higher resolving power for imaging the SVs and their densely packed molecular cargo. Moreover, during fusion, synaptotagmin remains clustered inside the vesicles; that is, it does not diffuse to the plasma membrane after exocytosis [56].

### 5.4. 3D nanoscale neuronal imaging

Fluorescence nanoscopy has already paved the way for neural circuit imaging with nanoscale spatial resolution. Using STORM, neuronal structure mapping of retinal ganglion cells has been projected in three dimensions, providing synaptic connectivity at the

neural circuit scale [57]. In Fig. 5(a) [57], a retinal ganglion cell (blue), postsynaptic scaffolding protein gephyrin (green), and presynaptic proteins (magenta) were imaged using STORM [57]. Using STED microscopy, the dendritic and axonal structures of enhanced yellow fluorescent protein (eYFP)-labeled neurons from the molecular layer of the somatosensory cortex of a mouse were observed *in vivo* [58]; the projected volumes of the fine neural structures and the temporal dynamics of spine morphology were revealed with a spatial resolution of 67 nm (Fig. 5(b) [58]). In addition, by combining Bessel beam SIM (BB-SIM) and the tissue-clearing method, the localization and abundance of single messenger RNAs (mRNAs) (single-molecule fluorescence *in situ* hybridization (smFISH)) can be identified in whole-mount adult *Drosophila* brains [59].

## 6. Future research directions

### 6.1. MINFLUX nanoscopy

Sometimes referred to as the “post-Nobel” fluorescence nanoscopic technique, MINFLUX nanoscopy has already opened a new avenue of research in understanding the protein structure and function of neurons, in both fixed and living cells [16]. A potential application of MINFLUX nanoscopy is to determine synaptic parameters and visualize synaptic plasticity. Determining synaptic parameters requires quantification modeling during vesicle fusion or neurotransmitter release with nanometer spatial resolution and microsecond temporal resolution. Long-term changes that last for hours or longer provide a physiological substrate for learning and memory, whereas short-term changes that occur in time periods of milliseconds to minutes. MINFLUX nanoscopy provides ultra-high spatiotemporal resolution and long-term live-cell tracking and imaging abilities that enable precise synaptic parameter modeling and synaptic plasticity visualization with decreased phototoxicity. Furthermore, combined with high-resolution imaging through the physical sample expansion approach (ExM), a

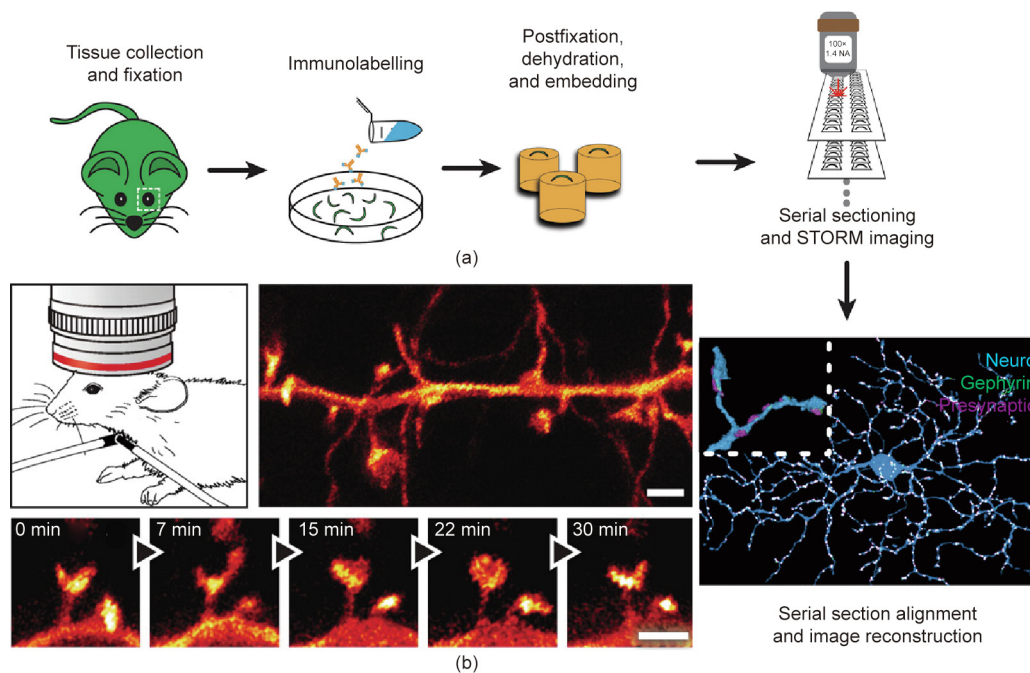


**Fig. 5.** Nanoscopic imaging of a neuron *ex vivo* and *in vivo*. (a) Sample preparation and *ex vivo* STORM imaging of a retinal ganglion cell. The inset of the final image (lower right) shows the magnified view of a dendrite section. (b) *In vivo* STED imaging of the somatosensory cortex of a mouse. (a) Reproduced from Ref. [57] with permission of Elsevier, © 2015; (b) reproduced from Ref. [58] with permission of The American Association for the Advancement of Science, © 2012.

multiple-fold increase in the spatial resolution of fluorescence nanoscopy, especially of MINFLUX nanoscopy, can potentially be achieved.

## 6.2. Fluorescent bioconjugates

The performance of fluorescence nanoscopy is closely related to the optical characteristics of fluorescent probes [60]. For example, a nanoscopic technique with high spatiotemporal resolution called “quick single molecule-guided Bayesian localization microscopy (quick-SIMBA)” has been developed using a new photoconvertible fluorescent protein (FP), pcStar, and has been used to discover a specific “parallel three-pillar” structure of the neuronal-glia cell junction in *Drosophila* embryos [61]. In addition to endogenous fluorescent probes, that is, FPs, new exogenous probes are being developed to increase image brightness, improve spatial resolution, and enhance the specificity of labeling in fluorescence nanoscopy, including small molecule organic dyes [62], quantum dots [63], aggregation-induced emission nanoparticles [64], polymer dots [65], and up-conversion nanoparticles (UCNPs) [66]. The development of new fluorescent probe bioconjugates with smaller sizes and improved efficiencies has the potential to lead to further advances in the imaging resolution of fluorescence nanoscopy. Furthermore, using the stochastic binding of dye-labeled deoxyribonucleic acid (DNA) probes, DNA-PAINT achieved similar image resolution on DNA-origami nanostructures [67,68]. It is worth mentioning that exchangeable fluorophores have been successfully adopted for use with STED, as STED-PAINT [69].

## 6.3. Genomic imaging

The normal function of a neuron is based on the collective action of many types of molecules. However, the spectral overlap between fluorophores limits the number of molecular species that can be measured simultaneously. Recently developed genomic-scale imaging techniques based on multiplexed fluorescence *in situ* hybridization (FISH) greatly increase the number of molecular species that can be imaged simultaneously with a certain error tolerance. For example, a specially designed multiple-bit binary word can be encoded into the fluorescent probe during the labeling of RNA molecules, which can be probed according to the codebook. Single-cell transcriptome imaging methods have realized the imaging and multiplexing of more than 1000 genes in a single cell via *in situ* sequencing [70,71] and FISH [72–74]. The combination of these techniques with fluorescence nanoscopy could potentially provide new insights into the structures and functions of neurons at the molecular level.

## 6.4. Optical tools and other related imaging techniques

### 6.4.1. Optogenetics

Fluorescence nanoscopy is an important tool for studying the dynamic processes inside and between neurons, which involve the fast and precise control of specific cells in the brain while leaving others unaltered. The precision of electrodes is not high enough, and drugs act much too slowly. Optogenetics is a technology that combines genetic and optical methods to activate or inhibit well-defined events in specific cells of living tissue [75]. However, the penetration depth of visible light is limited by strong scattering by endogenous chromophores [75]. Near-infrared (NIR) light has a deeper penetration depth in biological tissue, but its wavelengths lie outside the optogenetic window. UCNPs can convert low-energy incident NIR photons into high-energy visible emission, and the spectrum can be tuned to accommodate different light-activated channels [76]. Combining fluorescence nano-

scopy with UCNP-mediated optogenetics offers exciting possibilities for invasive study of the controlled neuronal activity deep inside the brain.

### 6.4.2. Direct laser writing of neuron-like structures

Can we print the mind? This is a fascinating question. However, the complexity of the brain is beyond the ability of conventional fabrication techniques. Combined with direct laser writing, fluorescence nanoscopy could boost the development of bionic photonic chips that mimic brain functions more closely. Two-photon direct laser writing has produced 3D biomimetic neuron structures of various topologies with sub-micrometer features [77], and two-beam laser writing can fabricate structures with features as small as 9 nm [78].

### 6.4.3. Related imaging techniques

The measurement of APs is of significant importance in neuroscience. At present, electrophysiology using patch-clamping is the gold standard for the measurement of individual APs. However, although it has an excellent temporal resolution and a good signal-to-noise ratio, the spatial resolution is limited to approximately 10  $\mu\text{m}$ . The photoluminescence of nitrogen-vacancy (NV) centers varies with the magnetic field generated by the propagation of APs in a process called optically detected magnetic resonance (ODMR). This enables high-resolution magnetic field sensing in biological systems under ambient conditions [79,80]. For example, detection of the AP in single neurons and intact organisms has been demonstrated using ODMR [81]. By combining fluorescence nanoscopy with ODMR, APs with the strength changes of synapses could be visualized and measured at nanoscale spatial resolution.

The imaging depth in brain tissue is limited principally by strong light absorption and scattering in the visible range, making it difficult to resolve images from deeper layers in the brain, even in small animals. A direct way to tackle this problem is to access the targeted deep region by inserting a gradient-index (GRIN) lens [82] or fiberscopes [83], or by using a microprism [84]. For example, a vertical cross-section of the tissue can be imaged using a microprism [84]. GRIN lenses have been used to image deep brain tissue, including the hippocampus, hypothalamus, thalamus, and fine structures such as dendritic spines in the CA1 hippocampus [85]. The spatial resolution of these techniques is limited; therefore, incorporating fluorescence nanoscopy could help in realizing all-scale deep-brain imaging.

To improve the penetration depth by reducing light absorption, multi-photon microscopy (MPM) uses excitations of longer wavelengths. The imaging depth of three-photon fluorescence has been shown to be 5–6 effective attenuation lengths below the surface of mouse brain tissue, which is around 130  $\mu\text{m}$  for 755 nm excitation [86]. Furthermore, imaging depths ranging from 1.2–1.6 mm beneath the mouse brain surface have been achieved using two-photon fluorescence with 1280 nm excitations [87,88]. Coherent Raman scattering (CRS), such as stimulated Raman scattering (SRS) and coherent anti-Stokes Raman scattering, is another MPM technique for deep-tissue imaging. SRS has been used to detect and image membrane potential distributions at both the subcellular and multi-neuron scales [89,90] and to image the neurotransmitter acetylcholine at neuromuscular junctions [91]. Although the spatial resolution of CRS is limited by light diffraction, methods based on tip-enhanced CRS [92,93], the suppression or saturation of CRS [94–96], and high-order nonlinear processes [97] have been developed to navigate this problem. Future CRS developments may realize imaging at the nanometer scale and provide information complementary to that of fluorescence nanoscopy.

In addition to light absorption, light scattering is another issue that limits imaging depth, as it introduces aberration into the

imaging process. Adaptive optics (AO) uses active devices, such as deformable mirrors and liquid crystal spatial light modulators (SLMs), to compensate for wavefront distortion, which can be measured directly [98] or indirectly [99]. AO has been applied in single-molecule localization microscopy (e.g., PALM and STORM) [100,101], SIM [102], and STED microscopy [103], resulting in significant improvements in localization accuracy, image sharpness, and brightness. It is anticipated that new research on AO will continue to contribute to advances in fluorescence nanoscopy, including MINFLUX nanoscopy.

The combination of machine learning (ML) and fluorescence nanoscopy offers another research direction. Recently, ML has been applied in optical imaging through scattering media [104], which may be useful for deep-brain imaging. ML has also been used to speed up data processing in STORM [105] and to improve the spatial resolution of imaging [106]. Furthermore, ML can be combined with optically digitalized holography (ODH) to enable the on-demand tailoring of excitation field vectors [107], which could enhance the flexibility of fluorescence nanoscopy. With the development of photonic memristors, in which optical properties change in accordance with the transmitted light [108], it is possible to fabricate dynamic ODH for all-optical neuromorphic computing [109–111] and high-speed nanoscopic imaging.

## 7. Conclusions

Having developed at a rapid pace over the last few decades, fluorescence nanoscopy research is expected to spur further advancements in fluorescence probes and labeling methods to achieve ultrahigh resolution imaging, while reducing the required photon budget and the phototoxicity of samples. Unlike conventional microscopy, fluorescence nanoscopy provides a promising means of achieving genomic-scale imaging, which will yield a comprehensive picture of the molecular basis of cellular behaviors and functions. Combined with other optical methods, precise modeling, and the manipulation of neural activity in the deep brain, fluorescence nanoscopy will continue to revolutionize neuroscience. MINFLUX nanoscopy will enable *in vivo* imaging and the tracking of neural activity to further quantify synaptic parameters with nanometer spatial resolution and microsecond temporal resolution. ML-based fluorescence nanoscopy has the potential to deliver unprecedented application developments in neuroscience. Due to their immense promise, all forms of fluorescence nanoscopy will continue to elucidate the secrets of the brain and contribute to breakthrough developments in artificial intelligence.

## Acknowledgments

Min Gu acknowledges funding support from the Zhangjiang National Innovation Demonstration Zone (ZJ2019-ZD-005). Jian Lin acknowledges funding support from the National Natural Science Foundation of China (11874267). Yangyundou Wang is supported by a fellowship of the China Postdoctoral Science Foundation (2020M671169).

## Compliance with ethics guidelines

Yangyundou Wang, Jian Lin, Qiming Zhang, Xi Chen, Haitao Luan, and Min Gu declare that they have no conflict of interest or financial conflicts to disclose.

## References

[1] Purves D, Augustine GJ, Fitzpatrick D, Hall WC, Lamantia AS, McNamara JO, et al. *Neuroscience*. 3rd ed. Massachusetts: Sinauer Associates Inc Publishers; 2004.

[2] Zhou Q, Lai Y, Bacaj T, Zhao M, Lyubimov AY, Uervirojnangkoorn M, et al. Architecture of the synaptotagmin–SNARE machinery for neuronal exocytosis. *Nature* 2015;525(7567):62–7.

[3] Südhof TC, Rothman JE. Membrane fusion: grappling with SNARE and SM proteins. *Science* 2009;323(5913):474–7.

[4] Hinrichsen L, Meyerholz A, Groos S, Ungewickell EJ. Bending a membrane: how clathrin affects budding. *Proc Natl Acad Sci USA* 2006;103(23):8715–20.

[5] Thanawala MS, Regehr WG. Determining synaptic parameters using high-frequency activation. *J Neurosci Methods* 2016;264:136–52.

[6] Gustafsson MGL. Surpassing the lateral resolution limit by a factor of two using structured illumination microscopy. *J Microsc* 2000;198(2):82–7.

[7] Gustafsson MGL, Shao L, Carlton PM, Wang CJR, Golubovskaya IN, Cande WZ, et al. Three-dimensional resolution doubling in wide-field fluorescence microscopy by structured illumination. *Biophys J* 2008;94(12):4957–70.

[8] Schermelleh L, Carlton PM, Haase S, Shao L, Winoto L, Kner P, et al. Subdiffraction multicolor imaging of the nuclear periphery with 3D structured illumination microscopy. *Science* 2008;320(5881):1332–6.

[9] Hell SW, Wichmann J. Breaking the diffraction resolution limit by stimulated emission: stimulated-emission-depletion fluorescence microscopy. *Opt Lett* 1994;19(11):780–2.

[10] Hell SW, Kroug M. Ground-state-depletion fluorescence microscopy: a concept for breaking the diffraction resolution limit. *Appl Phys B* 1995;60(5):495–7.

[11] Rust MJ, Bates M, Zhuang X. Sub-diffraction-limit imaging by stochastic optical reconstruction microscopy (STORM). *Nat Methods* 2006;3(10):793–6.

[12] Betzig E, Patterson GH, Sougrat R, Lindwasser OW, Olenych S, Bonifacino JS, et al. Imaging intracellular fluorescent proteins at nanometer resolution. *Science* 2006;313(5793):1642–5.

[13] Hess ST, Girirajan TPK, Mason MD. Ultra-high resolution imaging by fluorescence photoactivation localization microscopy. *Biophys J* 2006;91(11):4258–72.

[14] Balzarotti F, Eilers Y, Gwosch KC, Gynnà AH, Westphal V, Stefani FD, et al. Nanometer resolution imaging and tracking of fluorescent molecules with minimal photon fluxes. *Science* 2017;355(6325):606–12.

[15] Eilers Y, Ta H, Gwosch KC, Balzarotti F, Hell SW. MINFLUX monitors rapid molecular jumps with superior spatiotemporal resolution. *Proc Natl Acad Sci USA* 2018;115(24):6117–22.

[16] Gwosch KC, Pape JK, Balzarotti F, Hoess P, Ellenberg J, Ries J, et al. MINFLUX nanoscopy delivers 3D multicolor nanometer resolution in cells. *Nat Methods* 2020;17(2):217–24.

[17] Sigal YM, Zhou R, Zhuang X. Visualizing and discovering cellular structures with super-resolution microscopy. *Science* 2018;361(6405):880–7.

[18] Valeur B, Berberan-Santos MN. *Molecular fluorescence: principles and applications*. 2nd ed. Weinheim: Wiley–VCH Verlag GmbH; 2012.

[19] Gu M. *Principles of three-dimensional imaging in confocal microscopes*. Singapore: World Scientific; 1996.

[20] Zipfel WR, Williams RM, Webb WW. Nonlinear magic: multiphoton microscopy in the biosciences. *Nat Biotechnol* 2003;21(11):1369–77.

[21] Gugel H, Bewersdorf J, Jakobs S, Engelhardt J, Storz R, Hell SW. Cooperative 4Pi excitation and detection yields sevenfold sharper optical sections in live-cell microscopy. *Biophys J* 2004;87(6):4146–52.

[22] Wang BK, Barbiero M, Zhang QM, Gu M. Super-resolution optical microscope: principle, instrumentation, and application. *Front Inf Technol Electron Eng* 2019;20(5):608–30.

[23] Chen F, Tillberg PW, Boyden ES. Optical imaging. Expansion microscopy. *Science* 2015;347(6221):543–8.

[24] Tillberg PW, Chen F, Piatkevich KD, Zhao Y, Yu CC, English BP, et al. Protein-retention expansion microscopy of cells and tissues labeled using standard fluorescent proteins and antibodies. *Nat Biotechnol* 2016;34(9):987–92.

[25] Chen F, Wassie AT, Cote AJ, Sinha A, Alon S, Asano S, et al. Nanoscale imaging of RNA with expansion microscopy. *Nat Methods* 2016;13(8):679–84.

[26] Zhao Y, Bucur O, Irshad H, Chen F, Weins A, Stancu AL, et al. Nanoscale imaging of clinical specimens using pathology-optimized expansion microscopy. *Nat Biotechnol* 2017;35(8):757–64.

[27] Murakami TC, Mano T, Saikawa S, Horiguchi SA, Shigeta D, Baba K, et al. A three-dimensional single-cell-resolution whole-brain atlas using CUBIC-X expansion microscopy and tissue clearing. *Nat Neurosci* 2018;21(4):625–37.

[28] Schneider J, Zahn J, Maglione M, Sigrist SJ, Marquard J, Chojnacki J, et al. Ultrafast, temporally stochastic STED nanoscopy of millisecond dynamics. *Nat Methods* 2015;12(9):827–30.

[29] Jones SA, Shim SH, He J, Zhuang X. Fast, three-dimensional super-resolution imaging of live cells. *Nat Methods* 2011;8(6):499–505.

[30] Huang F, Hartwich TMP, Rivera-Molina FE, Lin Y, Duim WC, Long JJ, et al. Video-rate nanoscopy using sCMOS camera-specific single-molecule localization algorithms. *Nat Methods* 2013;10(7):653–8.

[31] Li D, Shao L, Chen BC, Zhang X, Zhang M, Moses B, et al. Extended-resolution structured illumination imaging of endocytic and cytoskeletal dynamics. *Science* 2015;349(6251):aab3500.

[32] Ehmman N, Sauer M, Kittel RJ. Super-resolution microscopy of the synaptic active zone. *Front Cell Neurosci* 2015;9:7.

[33] Liu KSY, Siebert M, Mertel S, Knoche E, Wegener S, Wichmann C, et al. RIM-binding protein, a central part of the active zone, is essential for neurotransmitter release. *Science* 2011;334(6062):1565–9.

[34] Ehmman N, van de Linde S, Alon A, Ljaschenko D, Keung XZ, Holm T, et al. Quantitative super-resolution imaging of Bruchpilot distinguishes active zone states. *Nat Commun* 2014;5:4650.



- [35] Sieber JJ, Willig KI, Heintzmann R, Hell SW, Lang T. The SNARE motif is essential for the formation of syntaxin clusters in the plasma membrane. *Biophys J* 2006;90(8):2843–51.
- [36] Donnert G, Keller J, Medda R, Andrei MA, Rizzoli SO, Lührmann R, et al. Macromolecular-scale resolution in biological fluorescence microscopy. *Proc Natl Acad Sci USA* 2006;103(31):11440–5.
- [37] Kellner RR, Baier CJ, Willig KI, Hell SW, Barrantes FJ. Nanoscale organization of nicotinic acetylcholine receptors revealed by stimulated emission depletion microscopy. *Neuroscience* 2007;144(1):135–43.
- [38] Kornau H, Schenker L, Kennedy M, Seeburg P. Domain interaction between NMDA receptor subunits and the postsynaptic density protein PSD-95. *Science* 1995;269(5231):1737–40.
- [39] Kim E, Naisbitt S, Hsueh YP, Rao A, Rothschild A, Craig AM, et al. GKAP, a novel synaptic protein that interacts with the guanylate kinase-like domain of the PSD-95/SAP90 family of channel clustering molecules. *J Cell Biol* 1997;136(3):669–78.
- [40] Naisbitt S, Kim E, Tu JC, Xiao B, Sala C, Valtschanoff J, et al. Shank, a novel family of postsynaptic density proteins that binds to the NMDA receptor/PSD-95/GKAP complex and cortactin. *Neuron* 1999;23(3):569–82.
- [41] Xiao B, Tu JC, Petralia RS, Yuan JP, Doan A, Breder CD, et al. Homer regulates the association of group 1 metabotropic glutamate receptors with multivalent complexes of homer-related, synaptic proteins. *Neuron* 1998;21(4):707–16.
- [42] Dani A, Huang B, Bergan J, Dulac C, Zhuang X. Superresolution imaging of chemical synapses in the brain. *Neuron* 2010;68(5):843–56.
- [43] MacGillavry H, Song Y, Raghavachari S, Blanpied T. Nanoscale scaffolding domains within the postsynaptic density concentrate synaptic AMPA receptors. *Neuron* 2013;78(4):615–22.
- [44] Tang AH, Chen H, Li TP, Metzbowser SR, MacGillavry HD, Blanpied TA. A trans-synaptic nanocolumn aligns neurotransmitter release to receptors. *Nature* 2016;536(7615):210–4.
- [45] Fukata Y, Dimitrov A, Boncompain G, Vilemeyer O, Perez F, Fukata M. Local palmitoylation cycles define activity-regulated postsynaptic subdomains. *J Cell Biol* 2013;202(1):145–61.
- [46] Masch JM, Steffens H, Fischer J, Engelhardt J, Hubrich J, Keller-Findeisen J, et al. Robust nanoscopy of a synaptic protein in living mice by organic-fluorophore labeling. *Proc Natl Acad Sci USA* 2018;115(34):E8047–56.
- [47] Xu K, Zhong G, Zhuang X. Actin, spectrin, and associated proteins form a periodic cytoskeletal structure in axons. *Science* 2013;339(6118):452–6.
- [48] D'Este E, Kamin D, Göttfert F, El-Hady A, Hell S. STED nanoscopy reveals the ubiquity of subcortical cytoskeleton periodicity in living neurons. *Cell Rep* 2015;10(8):1246–51.
- [49] Zhong G, He J, Zhou R, Lorenzo D, Babcock HP, Bennett V, et al. Developmental mechanism of the periodic membrane skeleton in axons. *eLife* 2014;3:e04581.
- [50] Chierico L, Joseph AS, Lewis AL, Battaglia G. Live cell imaging of membrane/cytoskeleton interactions and membrane topology. *Sci Rep* 2014;4:6056.
- [51] Han B, Zhou R, Xia C, Zhuang X. Structural organization of the actin-spectrin-based membrane skeleton in dendrites and soma of neurons. *Proc Natl Acad Sci USA* 2017;114(32):E6678–85.
- [52] D'Este E, Kamin D, Velte C, Göttfert F, Simons M, Hell SW. Subcortical cytoskeleton periodicity throughout the nervous system. *Sci Rep* 2016;6:22741.
- [53] D'Este E, Kamin D, Balzarotti F, Hell SW. Ultrastructural anatomy of nodes of Ranvier in the peripheral nervous system as revealed by STED microscopy. *Proc Natl Acad Sci USA* 2017;114(2):E191–9.
- [54] Westphal V, Rizzoli SO, Lauterbach MA, Kamin D, Jahn R, Hell SW. Video-rate far-field optical nanoscopy dissects synaptic vesicle movement. *Science* 2008;320(5873):246–9.
- [55] Yeung C, Shtrahman M, Wu XL. Stick-and-diffuse and caged diffusion: a comparison of two models of synaptic vesicle dynamics. *Biophys J* 2007;92(7):2271–80.
- [56] Willig KI, Rizzoli SO, Westphal V, Jahn R, Hell SW. STED microscopy reveals that synaptotagmin remains clustered after synaptic vesicle exocytosis. *Nature* 2006;440(7086):935–9.
- [57] Sigal Y, Speer C, Babcock H, Zhuang X. Mapping synaptic input fields of neurons with super-resolution imaging. *Cell* 2015;163(2):493–505.
- [58] Berning S, Willig KI, Steffens H, Dibaj P, Hell SW. Nanoscopy in a living mouse brain. *Science* 2012;335(6068):551.
- [59] Long X, Colonell J, Wong AM, Singer RH, Lionnet T. Quantitative mRNA imaging throughout the entire *Drosophila* brain. *Nat Methods* 2017;14(7):703–6.
- [60] Wu Y, Ruan H, Dong Z, Zhao R, Yu J, Tang X, et al. Fluorescent polymer dot-based multicolor stimulated emission depletion nanoscopy with a single laser beam pair for cellular tracking. *Anal Chem* 2020;92(17):12088–96.
- [61] Zhang M, Fu Z, Li C, Liu A, Peng D, Xue F, et al. Fast super-resolution imaging technique and immediate early nanostructure capturing by a photoconvertible fluorescent protein. *Nano Lett* 2020;20(4):2197–208.
- [62] Ye Z, Yang W, Wang C, Zheng Y, Chi W, Liu X, et al. Quaternary piperazine-substituted rhodamines with enhanced brightness for super-resolution imaging. *J Am Chem Soc* 2019;141(37):14491–5.
- [63] Ye S, Guo J, Song J, Qu J. Achieving high-resolution of 21 nm for STED nanoscopy assisted by CdSe@ZnS quantum dots. *Appl Phys Lett* 2020;116(4):041101.
- [64] Li D, Ni X, Zhang X, Liu L, Qu J, Ding D, et al. Aggregation-induced emission luminogen-assisted stimulated emission depletion nanoscopy for super-resolution mitochondrial visualization in live cells. *Nano Res* 2018;11(11):6023–33.
- [65] Zhang Z, Fang X, Liu Z, Liu H, Chen D, He S, et al. Semiconducting polymer dots with dual-enhanced NIR-IIa fluorescence for through-skull mouse-brain imaging. *Angew Chem Int Ed Engl* 2020;59(9):3691–8.
- [66] Chen C, Wang F, Wen S, Su QP, Wu MCL, Liu Y, et al. Multi-photon near-infrared emission saturation nanoscopy using upconversion nanoparticles. *Nat Commun* 2018;9(1):3290.
- [67] Gu L, Li Y, Zhang S, Xue Y, Li W, Li D, et al. Molecular resolution imaging by repetitive optical selective exposure. *Nat Methods* 2019;16(11):1114–8.
- [68] Cnossen J, Hinsdale T, Thorsen RØ, Siemons M, Schueder F, Jungmann R, et al. Localization microscopy at doubled precision with patterned illumination. *Nat Methods* 2020;17(1):59–63.
- [69] Spahn C, Hurter F, Glaesmann M, Karathanasis C, Lampe M, Heilemann M. Protein-specific, multicolor and 3D STED imaging in cells with DNA-labeled antibodies. *Angew Chem Int Ed Engl* 2019;58(52):18835–8.
- [70] Wang X, Allen WE, Wright MA, Sylwestrak EL, Samusik N, Vesuna S, et al. Three-dimensional intact-tissue sequencing of single-cell transcriptional states. *Science* 2018;361(6400):eaat5691.
- [71] Lee JH, Daugharthy ER, Scheiman J, Kalhor R, Yang JL, Ferrante TC, et al. Highly multiplexed subcellular RNA sequencing *in situ*. *Science* 2014;343(6177):1360–3.
- [72] Chen KH, Boettiger AN, Moffitt JR, Wang S, Zhuang X. Spatially resolved, highly multiplexed RNA profiling in single cells. *Science* 2015;348(6233):aaa6090.
- [73] Shah S, Takei Y, Zhou W, Lubeck E, Yun J, Eng CHL, et al. Dynamics and spatial genomics of the nascent transcriptome by intron seqFISH. *Cell* 2018;174(2):363–76.e16.
- [74] Eng CHL, Lawson M, Zhu Q, Dries R, Koulina N, Takei Y, et al. Transcriptome-scale super-resolved imaging in tissues by RNA seqFISH+. *Nature* 2019;568(7751):235–9.
- [75] Deisseroth K. Optogenetics: 10 years of microbial opsins in neuroscience. *Nat Neurosci* 2015;18(9):1213–25.
- [76] Chen S, Weitmier AZ, Zeng X, He L, Wang X, Tao Y, et al. Near-infrared deep brain stimulation via upconversion nanoparticle-mediated optogenetics. *Science* 2018;359(6376):679–84.
- [77] Yu H, Zhang Q, Gu M. Three-dimensional direct laser writing of biomimetic neuron structures. *Opt Express* 2018;26(24):32111–7.
- [78] Gan Z, Cao Y, Evans RA, Gu M. Three-dimensional deep sub-diffraction optical beam lithography with 9 nm feature size. *Nat Commun* 2013;4:2061.
- [79] Gruber A, Dräbenstedt A, Tietz C, Fleury L, Wrachtrup J, von Borczyskowski C. Scanning confocal optical microscopy and magnetic resonance on single defect centers. *Science* 1997;276(5321):2012–4.
- [80] Barbiero M, Castelletto S, Gan X, Gu M. Spin-manipulated nanoscopy for single nitrogen-vacancy center localizations in nanodiamonds. *Light Sci Appl* 2017;6(11):e17085.
- [81] Barry JF, Turner MJ, Schloss JM, Glenn DR, Song Y, Lukin MD, et al. Optical magnetic detection of single-neuron action potentials using quantum defects in diamond. *Proc Natl Acad Sci USA* 2016;113(49):14133–8.
- [82] Levene MJ, Dombbeck DA, Kasischke KA, Molloy RP, Webb WW. *In vivo* multiphoton microscopy of deep brain tissue. *J Neurophysiol* 2004;91(4):1908–12.
- [83] Szabo V, Ventalon C, De Sars V, Bradley J, Emiliani V. Spatially selective holographic photoactivation and functional fluorescence imaging in freely behaving mice with a fiberscope. *Neuron* 2014;84(6):1157–69.
- [84] Low RJ, Gu Y, Tank DW. Cellular resolution optical access to brain regions in fissures: imaging medial prefrontal cortex and grid cells in entorhinal cortex. *Proc Natl Acad Sci USA* 2014;111(52):18739–44.
- [85] Attardo A, Fitzgerald JE, Schnitzer MJ. Impermanence of dendritic spines in live adult CA1 hippocampus. *Nature* 2015;523(7562):592–6.
- [86] Horton NG, Wang K, Kobat D, Clark CG, Wise FW, Schaffer CB, et al. *In vivo* three-photon microscopy of subcortical structures within an intact mouse brain. *Nat Photonics* 2013;7(3):205–9.
- [87] Kobat D, Durst ME, Nishimura N, Wong AW, Schaffer CB, Xu C. Deep tissue multiphoton microscopy using longer wavelength excitation. *Opt Express* 2009;17(16):13354–64.
- [88] Theer P, Denk W. On the fundamental imaging-depth limit in two-photon microscopy. *J Opt Soc Am A* 2006;23(12):3139–49.
- [89] Liu B, Lee HJ, Zhang D, Liao CS, Ji N, Xia Y, et al. Label-free spectroscopic detection of membrane potential using stimulated Raman scattering. *Appl Phys Lett* 2015;106(17):173704.
- [90] Lee HJ, Zhang D, Jiang Y, Wu X, Shih PY, Liao CS, et al. Label-free vibrational spectroscopic imaging of neuronal membrane potential. *J Phys Chem Lett* 2017;8(9):1932–6.
- [91] Fu D, Yang W, Xie XS. Label-free imaging of neurotransmitter acetylcholine at neuromuscular junctions with stimulated Raman scattering. *J Am Chem Soc* 2017;139(2):583–6.
- [92] Ichimura T, Hayazawa N, Hashimoto M, Inouye Y, Kawata S. Tip-enhanced coherent anti-Stokes Raman scattering for vibrational nanoimaging. *Phys Rev Lett* 2004;92(22):220801.

- [93] Lin J, Zi Jian Er K, Zheng W, Huang Z. Radially polarized tip-enhanced near-field coherent anti-Stokes Raman scattering microscopy for vibrational nano-imaging. *Appl Phys Lett* 2013;103(8):083705.
- [94] Gong L, Wang H. Breaking the diffraction limit by saturation in stimulated-Raman-scattering microscopy: a theoretical study. *Phys Rev A* 2014;90(1):013818.
- [95] Gong L, Wang H. Suppression of stimulated Raman scattering by an electromagnetically-induced-transparency-like scheme and its application for super-resolution microscopy. *Phys Rev A* 2015;92(2):023828.
- [96] Gong L, Zheng W, Ma Y, Huang Z. Saturated stimulated-Raman-scattering microscopy for far-field superresolution bioimaging. *Phys Rev Appl* 2019;11(3):034041.
- [97] Gong L, Zheng W, Ma Y, Huang Z. Higher-order coherent anti-Stokes Raman scattering microscopy realizes label-free super-resolution vibrational imaging. *Nat Photonics* 2020;14(2):115–22.
- [98] Ji N, Milkie DE, Betzig E. Adaptive optics via pupil segmentation for high-resolution imaging in biological tissues. *Nat Methods* 2010;7(2):141–7.
- [99] Booth MJ. Wavefront sensorless adaptive optics for large aberrations. *Opt Lett* 2007;32(1):5–7.
- [100] Burke D, Patton B, Huang F, Bewersdorf J, Booth MJ. Adaptive optics correction of specimen-induced aberrations in single-molecule switching microscopy. *Optica* 2015;2(2):177–85.
- [101] Tehrani KF, Xu J, Zhang Y, Shen P, Kner P. Adaptive optics stochastic optical reconstruction microscopy (AO-STORM) using a genetic algorithm. *Opt Express* 2015;23(10):13677–92.
- [102] Thomas B, Wolstenholme A, Chaudhari SN, Kipreos ET, Kner P. Enhanced resolution through thick tissue with structured illumination and adaptive optics. *J Biomed Opt* 2015;20(2):026006.
- [103] Lenz MO, Sinclair HG, Savell A, Clegg JH, Brown ACN, Davis DM, et al. 3D stimulated emission depletion microscopy with programmable aberration correction. *J Biophotonics* 2014;7(1–2):29–36.
- [104] Horisaki R, Takagi R, Tanida J. Learning-based imaging through scattering media. *Opt Express* 2016;24(13):13738–43.
- [105] Nehme E, Weiss LE, Michaeli T, Schechtman Y. Deep-STORM: super-resolution single-molecule microscopy by deep learning. *Optica* 2018;5(4):458–64.
- [106] Wang H, Rivenson Y, Jin Y, Wei Z, Gao R, Günaydin H, et al. Deep learning enables cross-modality super-resolution in fluorescence microscopy. *Nat Methods* 2019;16(1):103–10.
- [107] Ren H, Shao W, Li Y, Salim F, Gu M. Three-dimensional vectorial holography based on machine learning inverse design. *Sci Adv* 2020;6(16):eaaz4261.
- [108] Goi E, Zhang Q, Chen X, Luan H, Gu M. Perspective on photonic memristive neuromorphic computing. *PhotonIX* 2020;1(1):3.
- [109] Gu M, Fang X, Ren H, Goi E. Optically digitalized holography: a perspective for all-optical machine learning. *Engineering* 2019;5(3):363–5.
- [110] Zhang Q, Yu H, Barbiero M, Wang B, Gu M. Artificial neural networks enabled by nanophotonics. *Light Sci Appl* 2019;8:42.
- [111] Goi E, Chen X, Zhang Q, Cumming BP, Schoenhardt S, Luan H, et al. Nanoprinted high-neuron-density optical linear perceptrons performing near-infrared inference on a CMOS chip. *Light Sci Appl* 2021;10:40.